Characterization of damage mode II in compression-induced shear mortar prisms by acoustic emission technique

Tam Nguyen Tat

Abstract

Acoustic Emission Technique (AET) has been conducted to classifydamages in cementitious specimens by applying RA method indicated in RILEM TC 212-ACD. However, the disadvantage of this method is that the percentages of damage modes (tensile and shear mode) are not quantified. It is also a topic of interest for recent researchers. This paper presents the compression-induced shear experiment tests on three cement mortar prisms. After filtering the noise-related signals, RA methodwas executed to individual signalsto determine the damages proportion. The results showeda significant discrepancy between the two modes: tensile mode occupied in the specimens.

Key words: Acoustic Emission, damage classification, compression-induced shear, mortar, mode I, mode II, RA method

Dr. Tam Nguyen Tat
Faculty of Civil Engineering
Hanoi Architectural University
Tel: 0989664268

Date of receipt: 17/6/2024
Editing date: 20/6/2024
Post approval date: 04/11/2024

1. Introduction

AET is a common non-destructive testing method that used to locate the micro-cracks, characterize the damage modes, and assess the damage severity of the construction structures. Some primary AE parameters can be directly extracted from one signal such as the Count, Amplitude, Duration, Rise-time (Figure 1). And some secondary features as RA and AF are calculated as follow, the Rise-timeper maximum Amplitude resulted RA value (ms/V) while the Average Frequency (AF, kHz) is obtained from Count per Duration.It is believed that by damage classification applying RA method, the tensile mode (or mode I) results waveforms with short Rise-time and high AF, whereas shear mode (or mode II)generates waveforms with longerRise-time and lower AF than those in mode I[1].

The RA method was widely applied to classify damage modes in laboratory tests as well as in real-structure assessments as represented in some studies in [1], [2], [3], [4], [5], because the process of damage in tested material can be operated without moving the specimen and its heavily load above. However, this method has a disadvantage that users have to decide the proportion of mode I and mode II damages. To illustrate, the position of the diagonal line which divide the damage zones on Figure 2 needs to be defined by users. This means that the ratio K = A/B (ms/V×kHz-1) varies depending on the testing configurations as well as type of material used for the experiments and the users have to determine it. Therefore, additional researches need to develop to help users to quantify damage proportions.

In some recent bending tests, the increase of RA at the same timewith the downshift of AF have been concluded to be related to the shifting of damage modes from tensile to shear [3], [5]. Additionally, some authors indicated that the damage processes have the similarly trend that they began with mode I whereas mode II appeared at final failure and lead the samples to completely broken[3], [5], [7], [8], [9], [10], [11].

However, the AE signals are elastic waves whichgeneratefrom micro-cracks (or events) within materialand then propagate to the receiving sensors. And during traveling, their shapes are influenced by the heterogeneity of propagation medium, by interruption of existing cracks and etc. Thus, their calculated AE parameters (for example, RA and AF) also strong influencedand thensupplying wrong information to the damage classification by RA method.In cement-based materials, this phenomenon has been found in some recent studies in[12], [13], [14], andsomeauthors concluded that RA values significant increasedwhen the propagation distancesincreased[13], [15]. Therefore, damage classification should definitely incorporate with the propagation distance data since the RA and AF values that used to characterize damage modes may well differ as measured by sensors at different places. Thus, the application of RA method to damage classify of cement-based structures is still questionable.

In terms of signal processing, during AE tests, a large number of AE signals with inconsistent shapes and parameters which do not correspond to AE hits are obtained. Thus, filtering works have been conducted on this raw data to eliminate surrounding noise. As noted, worthy, the hits with low magnitude (Duration less than 10 µs and count less than 2) could be related to background noise.

In this paper, three compressive tests to promote shear damage (compression-induced shear) on cement mortar prisms were conducted. The damage classification by RA method was conducted to individual signals after filteringwith coefficient K = 1/10(ms/V×kHz-1).

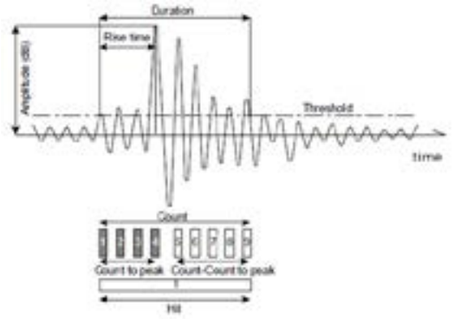

Figure 1. Conventional AE signal features[1]

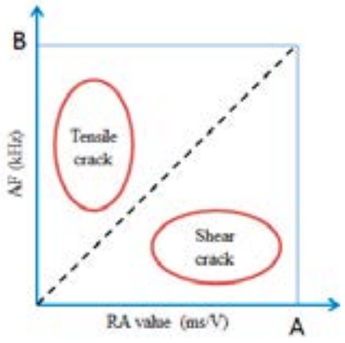

Figure 2. Damage classify by RA method in RILEM TC 212-ACD with the floating dash-line depends on RA and AF values [6]

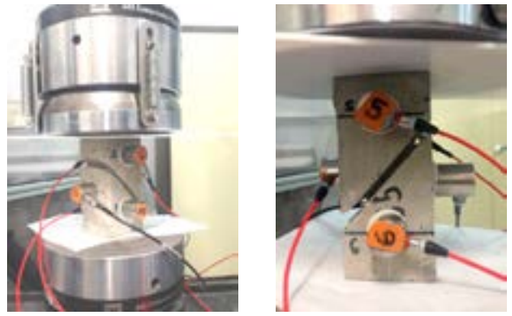

a) b)

Figure 3. Sensors arrangement on a) front and b) rear of specimens

2. Experimental methodology and acquirement system

2.1. Specimens' setup

Three mortar prisms, named MSC1, MSC2 and MSC3 (Mortar - Shearunder Compression-induced test), with dimensions of50×50×105 mm3were made. In thismaterial, the aggregates consist of 100% crush fine sand with maximum size less than 4 mm, and CEM I Portland cement(taken from Lafarge factory, France)was used. The sand/cement and water/cement ratio were 3.0 and 0.5, respectively. The mortar mechanical properties were determined at age of 28 days on threecylinder-specimens with diameter 118 mm and height 225 mm. The compressive strength, $f_c^{'} = 48.2$ MPa,and the Elastic modulus, E = 28.1 GPa,were calculated according to RILEM CPC8 recommendation.

The specimens were subjected to compression tests to promote shear failure on the 45-degree inclined diagonal surface under monotonic loading by a servo-hydraulic MTS machine. For that, notch with 4 mm in thickness and 15 mm in depth were practise as illustrated in Figure 2a and b. To control the test, a loading-rate of 50 N/s was applied.

2.2. Acoustic Emission acquisition setup

AE activities were recorded by using eight-channel PCI–8 acquisition device of the Physical Acoustic Corporation (PAC). AE detection was performed by means of six PAC R15-α sensors, with operating frequency from 50 to 400 kHz and resonant frequency 150 kHz. These sensors were fixed on the front-view and back-view of the samples as presented in Figure 3a) and b), respectively. The three-dimension Cartesian coordinates of the sensors are indicated in Table 1.

Table 1. AE sensors arrangement on specimens

Sensor no.	X (cm)	Y (cm)	Z (cm)
1	2.5	5.5	5.0
2	0	8.5	2.5
3	0	2.5	2.5
4	2.5	5.0	0
5	5.0	8.5	2.5
6	5.0	2.5	2.5

The PAC preamplifiers model 2/4/6 (selectable gain 20/40/60 dB + 5% dB) provide a gain of 40 dBs to increase the signal-to-noise ratio. The acquisition system was calibrated before each test using a standard source

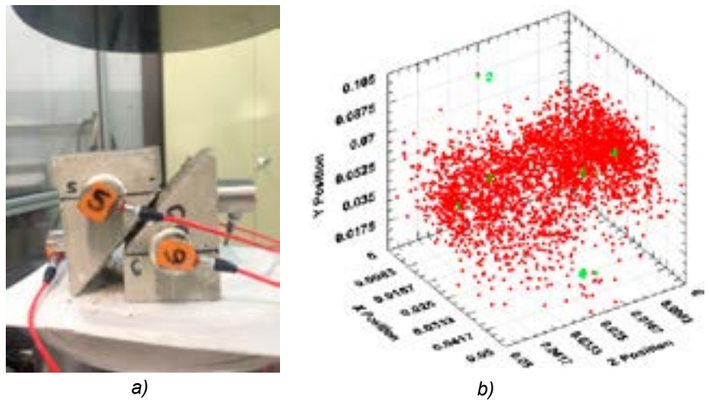

a) b)

Figure 4. Prism MSC3: a) Completely damagedat final and, b) 3D localization of AE events

Pencil Lead Break (PLB) procedure called Hsu-Nielsen test. To assure the changeless concerning sensors sensitivity before and after each test, an Auto Sensor Test (AST) was carried out. From the coupling tests (PLB and AST), the average velocity of acoustic wave propagation was estimated around 4,000 m/s for event localization.

3. Evolution of mechanical damage versus AE signals

During the tests, the initial AE events occur at the contact site between the platen of compressor machine and the sample surface. To reduce as possible, the occurrence of these events in order to limit frictions between the platens and the sample and to focus the damage progression around the notch position, two Teflon sheets were placed at both ends of the sample at the compressed-contact position. The Figure 4 a) and b) present the final failure of MSC3 specimen (MSC3 is chosen for illustration) and the location of the AE events obtained during the test, respectively.

Figure 5 shows the evolution of loading versus shortening displacement for three tested prisms. Globally, the three specimens presented the same trend. In MSC1, the peak loading value (25.5 kN) was archived for a shortening displacement of 656µm while in MSC2 and MSC3, the maximum load peak (23.7 kN and 23.8 kN) was reached for displacement values of 494 µm and 683 µm, respectively.

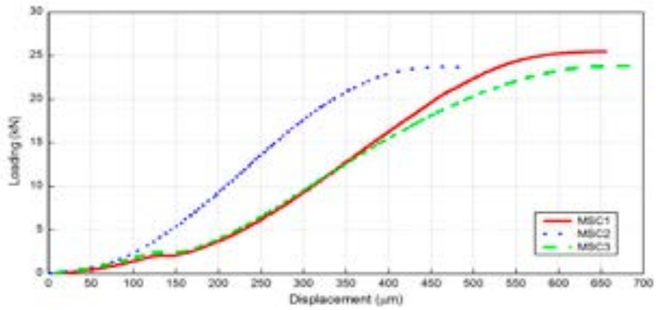

Figure 5. Evolution of loading and shortening displacementin MSC1, MSC2 and MSC3

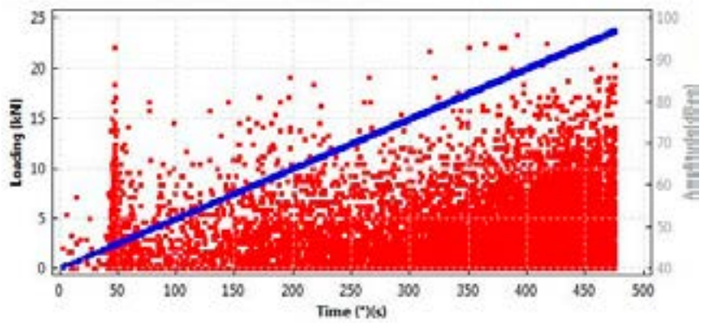

Figure 6. Loading and AE Amplitude versus time in MSC3

The Figure 6shows the loading curve and the Amplitude of signals obtained versus time in the MSC3 (MSC3 was chosen for illustration). During the test, AE signals were continuously recorded in the area around the notch. Before a crack became visible, a large number of micro-damages were created in the specimens. These micro-damages then lead to the visible crack at the notch position. In these tests, beams MSC1 generated 78,686 signals after 509 s; MSC2 and MSC3 received 30,826 signals (after 473 s) and 91,881 signals (after 475 s), respectively. It can be seen, MSC2 received the lowest number of AE signals comparing to MSC1 and MSC3. It could be explained that due to the lowest displacement of this specimen, the number of micro-cracks in MSC2 is lowest leading to the lowest number of AE signals.

The amount of received AE signals during MSC1, MSC2 and MSC3 testswere also represented by cumulative curves as shown inFigure 7,Figure 8andFigure 9, respectively. It has been observed that the number of AE signals is continuously increased parallel with the development of the loading, and almost signals were recorded in the period from 40% to peak load, as the appearance of the clearance steps in the final period of cumulative curves.

Figure 7, Figure 8 and Figure 9 present loading and cumulative of AE signals versus time during MSC1, MSC2 and MSC3 tests, respectively. It can be observed that the number of AE hits continuously increases with the development of the loading. And there is a change of kinetics at around loading value 15 kN (60% of peak load) at the time 300 s. From this point onward, the AE numbers are significantly increased.

4. Raw data filtering and clustering technique

Filtering process is necessary to distinguish AE signals from other interfering signals such as noise, friction between specimens and platen of testing machine and echo. In this study, signals with Count number less than 2 and Duration less than 10 µs was removed. A typical AE waveform removed from AE raw data by the filtering process is presented in Figure 10. The filtering results for three specimens are indicated in Table 2.

The Figure 10a) and b) illustrate the location of events before and after applying the filter technique for beam MSC3 at the failure state. The filtering technique had mostly eliminated the events localized far from the damaged zone.

5. Crack classification by applying RA method

In this study, an attempt to discriminate the damage modes (mode I or mode II damage) by means of a parametrical analysis (RA method) was made. According to the RILEM TC 212-ACD recommendation [6], the RA and AF values of the individual signal not eliminated after applying the noise filtering process are put on the same graph.

The maximum value on the RA and AF axis are A (ms/V) and B (kHz), respectively (Figure 2). The transition from mode I (or tensile mode) to mode II (or shear mode) at the ratio of K = A/B (ms/V×kHz-1) is indicated by the diagonal line on the classification diagram. In this diagram, the signal with high RA is classified to shear mode, whereas the signal with low RA is classified to tensile mode. The proportion of damage modes can thus be obtained.

In these tests, the maximum RA and AF values are 50 ms/V and 500 kHz, respectively, then demarcation line is defined with ratio K = 50/500 = 1/10 (ms/V×kHz-1). By applying RA method, the damage in MSC1, MSC2 and MSC3 was characterized by the dominance of tensile mode, as 96.8%, 96.3% and 97.3% of the whole damages, as presented in Figure 12, Figure 13 and Figure 14, respectively. The “strong” classes with high Amplitude, Duration and ABEN produced 100% tensile mode. And the other classes (0 and 1) having low Amplitude (from 40 to 50 dB) resulted in almost mode I and only 3.2% of mode II. At the end of the test, the MSC1 specimen was completely broken but no significant evolution of RA value was observed. This observation is contrary with what was reported in [3], [5], [7], [8], [9], [10], [11], where authors concluded that a large amount of signals with high RA appeared at the end of the test, before the fully failure of the specimens. Nevertheless, this conclusion was obtained on bending tests of concrete, RC and composite beams, while in this study we have tried to generate pure shear failure.

The same conclusions as in the case of MSC1 can be drawn for MSC2 and MSC3 in theFigure 13andFigure 14, respectively.

Damage classification by applying RA and AF that calculated from individual signals after noise-related filtering shows 100% signals in high-Amp group are classified to mode I. And almost of the signals in medium-Amp group are also assigned to tensile mode. The mode II is only classified from low-Amp group and it occupies around 3% of the whole signals. Most of the signals in mode II appear at the final moment of the tests and before the completely failure of specimens. However, the low amount of mode II in the shear-failure specimens under these tests raises a question to the damage classification by RA method.

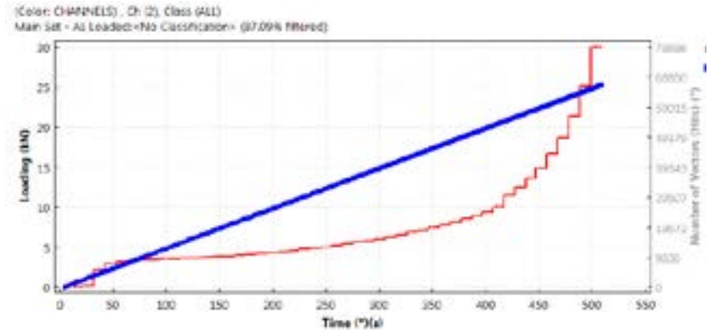

Figure 7. Evolution of loading and cumulative AE signals vs. time in MSC1

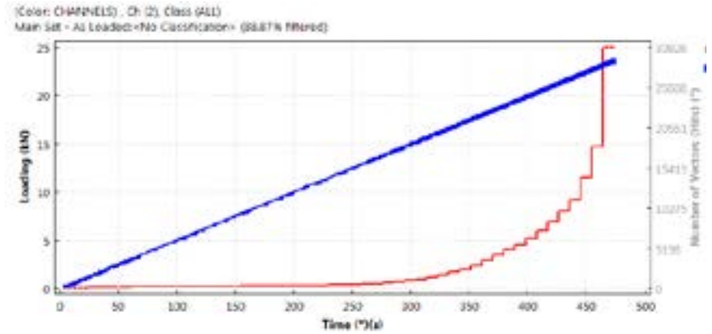

Figure 8. Evolution of loading and cumulative AE signals vs. time in MSC2

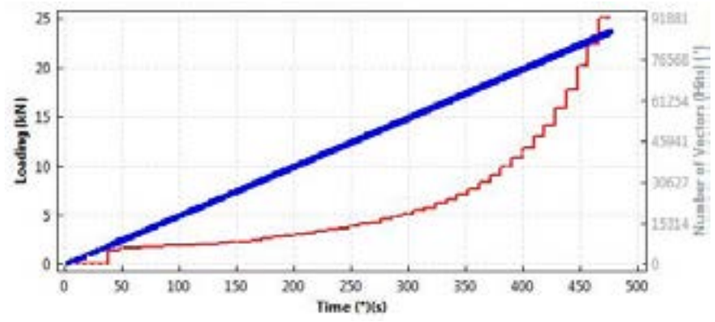

Figure 9. Evolution of loading and cumulative AE signals vs. time in MSC3

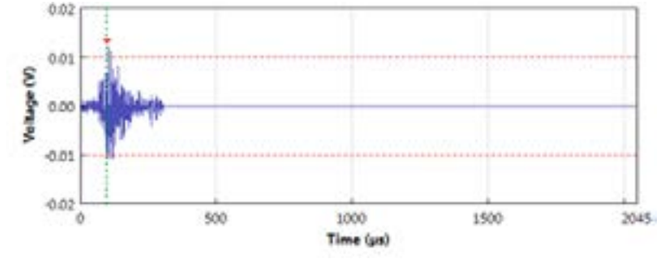

Figure 10. Noise-related signal illustration (Duration = 9 µs; Count = 3)

6. Conclusions

Background noise-related filtering technique applied to raw AE data plays an important role in the applications of RA method. Filtering processes preserved burst emission signals, thus resulting more accurately to damage classification. In this study, the filtering process eliminated up to 55% of the noise-related signals.

Table 2. Results of filtering noise-related signals

Beam	Number of Raw signals	Number of preserved signals	Proportion of noise-related signals (%)
MSC1	78,686	35,428	55%
MSC2	30,826	12,937	58%
MSC3	91,881	42,567	54%

It can be concluded that while 100% signals having high amplitude (above 65 dB) were assigned to mode I damage, the low-amplitude signals (40-55 dB) were assigned to both damage modes where the mode II occupied very low proportion. Results of damage classification on individual signals (i) indicated that mode I damage was dominant in three blocks. Although the specimens were completely failed, the low proportion of mode II was not in agreement with what has been reported in [3], [5], [7], [8], [9], [10], [11], where authors concluded that a large amount (they did not indicate the proportion) of signals having high RA values appeared at the end of the test and before the specimens are completely failed.

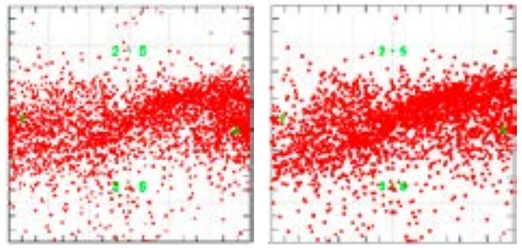

a) *b)*

Figure 11. 2D localization of events in MSC3: a) before, and b) after filteringthe noise-related signals

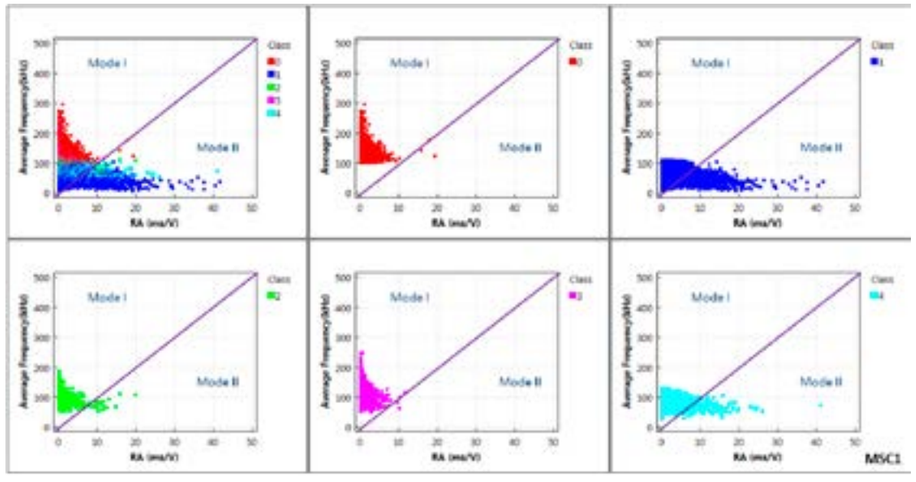

Figure 12. Damage classification in MSC1 specimen (K = 1/10), mode I: 96.8%

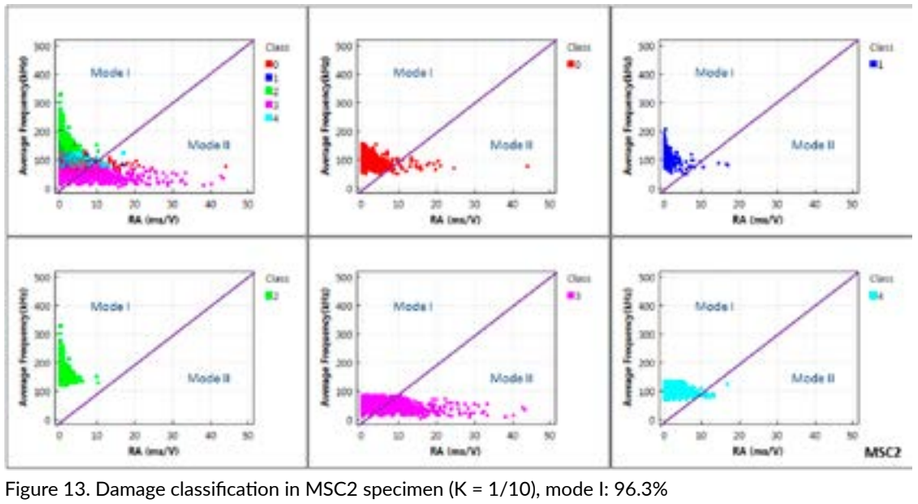

Figure 13. Damage classification in MSC2 specimen (K = 1/10), mode I: 96.3%

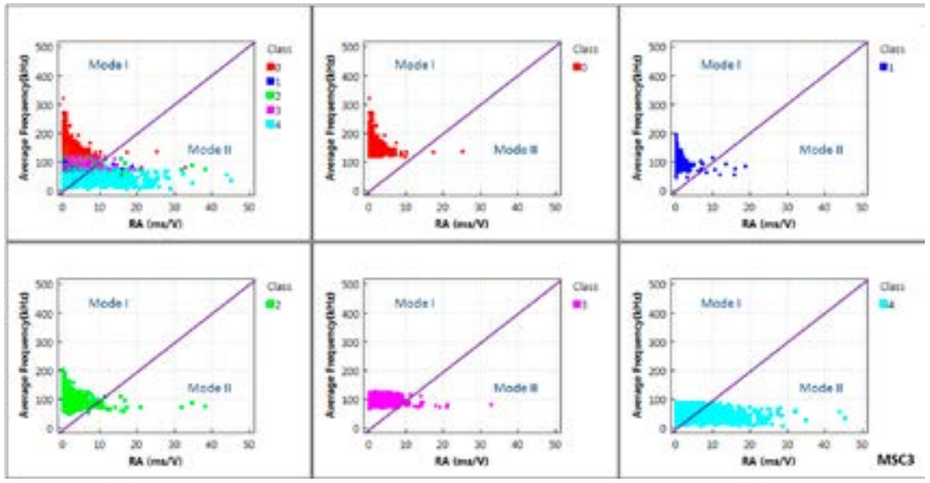

Figure 14. Damage classification in MSC3 specimen (K = 1/10), mode I: 97.3%

In terms of waveform shape of thesignals in mode II, it can be explained thatsome AE signals, which were affected by the development of crack in the specimen and etc., were converted to distortional waveforms with high RA. They appeared at the final moment when the cracks were accumulated in the specimens. These signals should be removed from the AE data before conducting the damage classification because they could introduce the wrong information. Thus, by eliminating these types of waveforms, the mode II does not exist./.

References

1. *D.G. Aggelis, D.V. Soulioti, N.M. Barkoula, A.S. Paipetis, and T.E. Matikas, "Influence of fiber chemical coating on the acoustic emission behavior of steel fiber reinforced concrete," Cem. Concr. Compos., vol. 34, no. 1, pp. 62–67, 2011, doi: 10.1016/j.cemconcomp.2011.07.003.*
2. *M.N. Noorsuhada, "An overview on fatigue damage assessment of reinforced concrete structures with the aid of acoustic emission technique," Constr. Build. Mater., vol. 112, pp. 424–439, Jun. 2016, doi: 10.1016/j.conbuildmat.2016.02.206.*
3. *Shigenori Yuyama, Zheng-wang Li, Yoshihiro Ito, and Masaki Arazoe, "Quantitative analysis of fracture process in RC column foundation by moment tensor analysis of acoustic emission," Constr. Build. Mater., vol. 13, no. 1, pp. 87–97, 1999.*
4. *K. Ohno and M. Ohtsu, "Crack classification in concrete based on acoustic emission," Constr. Build. Mater., vol. 24, no. 12, pp. 2339–2346, Dec. 2010, doi: 10.1016/j.conbuildmat.2010.05.004.*
5. *D. G. Aggelis, A. C. Mpalaskas, and T. E. Matikas, "Investigation of different fracture modes in cement-based materials by acoustic emission," Cem. Concr. Res., vol. 48, pp. 1–8, Jun. 2013, doi: 10.1016/j.cemconres.2013.02.002.*
6. *RILEM Technical Committee, "Recommendation of RILEM TC 212-ACD: acoustic emission and related NDE techniques for crack detection and damage evaluation in concrete: Test method for classification of active cracks in concrete structures by acoustic emission," Mater. Struct., vol. 43, no. 9, pp. 1187–1189, Nov. 2010, doi: 10.1617/s11527-010-9640-6.*
7. *A. Farhidzadeh, S. Salamone, and P. Singla, "A probabilistic approach for damage identification and crack mode classification in reinforced concrete structures," J. Intell. Mater. Syst. Struct., vol. 24, no. 14, pp. 1722–1735, Sep. 2013, doi: 10.1177/1045389X13484101.*
8. *Arash Behnia, Hwa Kian Chai, and Tomoki Shiotani, "Advanced structural health monitoring of concrete structures with the aid of acoustic emission," Constr. Build. Mater., vol. 65, pp. 282–302, Aug. 2014, doi: 10.1016/j.conbuildmat.2014.04.103.*
9. *A. Behnia, H. K. Chai, M. Yorikawa, S. Momoki, M. Terazawa, and T. Shiotani, "Integrated non-destructive assessment of concrete structures under flexure by acoustic emission and travel time tomography," Constr. Build. Mater., vol. 67, pp. 202–215, Sep. 2014, doi: 10.1016/j.conbuildmat.2014.05.011.*
10. *N. Ranjbar, A. Behnia, H. K. Chai, U. J. Alengaram, and M. Z. Jumaat, "Fracture evaluation of multi-layered precast reinforced geopolymer-concrete composite beams by incorporating acoustic emission into mechanical analysis," Constr. Build. Mater., vol. 127, pp. 274–283, Nov. 2016, doi: 10.1016/j.conbuildmat.2016.09.144.*
11. *A. Behnia, N. Ranjbar, H. K. Chai, Aziz. I. Abdullah, and M. Masaeli, "Fracture characterization of multi-layer wire mesh rubberized ferrocement composite slabs by means of acoustic emission," J. Clean. Prod., vol. 157, pp. 134–147, Jul. 2017, doi: 10.1016/j.jclepro.2017.03.192.*
12. *D.G. Aggelis, M. El Kadi, T. Tysmans, and J. Blom, "Effect of propagation distance on acoustic emission fracture mode classification in textile reinforced cement," Constr. Build. Mater., vol. 152, pp. 872–879, Oct. 2017, doi: 10.1016/j.conbuildmat.2017.06.166.*
13. *D.G. Aggelis, A.C. Mpalaskas, D. Ntalakas, and T.E. Matikas, "Effect of wave distortion on acoustic emission characterization of cementitious materials," Constr. Build. Mater., vol. 35, pp. 183–190, Oct. 2012, doi: 10.1016/j.conbuildmat.2012.03.013.*
14. *Fengqiao Zhang, "Evaluation of Acoustic Emission monitoring of existing concrete structures," Delft University of Technology, 2017.*
15. *D. Polyzos, A. Papacharalampopoulos, T. Shiotani, and D. G. Aggelis, "Dependence of AE parameters on the propagation distance," J Acoust Emiss, vol. 29, pp. 57–67, 2011.*